

Article

The Damage Evolution of a Cr₂O₃-TiO₂ Coating Subjected to Cyclic Impact and Corrosive Environments and the Influence of a Nickel Intermediate Layer

Huaxing Yang¹, Yang Zhao², Xudong Qin¹, Yixin Jin¹, Xinyang Zhao¹, Kailin Tian¹, Xiaoming Wang^{2,*} and Zhao Zhang^{1,*} 

¹ College of Electromechanical and Automotive Engineering, Yantai University, Yantai 264000, China

² Army Academy of Armored Forces, Beijing 100000, China

* Correspondence: uwangxm@126.com (X.W.); trojanz@yeah.net (Z.Z.)

Abstract: Cyclic impacts in corrosive environments significantly affect the service life of ceramic coatings, greatly increasing their susceptibility to cracking and delamination. This study investigated the damage evolution behavior of Cr₂O₃-TiO₂ (CT) coatings under cyclic stress in a corrosive medium, and analyzed the effects of the nickel layer on coating stress, corrosion current, and crack propagation. The variations in corrosion potential and current were analyzed, and the formation patterns of interfacial corrosion cracks were observed. Pre-cracks were introduced on the ceramic coating surface using a Micro-Nano mechanical testing system, and cyclic impacts were applied to the samples in 5% diluted hydrochloric acid using SiC balls to induce damage evolution. The results indicate that the presence of the nickel interlayer reduced the corrosion current density from 9.197×10^{-6} A/cm² to 8.088×10^{-6} A/cm² and significantly decreased the stress between the coating and the substrate. The surface cracks gradually extended toward the interface under the coupling effect of corrosion and SiC ball impact. When cracks reached the interface, they provided channels for corrosive media, leading to stress corrosion cracking at the interface. The Ni intermediate layer suppressed the formation of interface cracks and greatly enhanced the impact damage resistance of the CT coating–substrate system in corrosive media.

Keywords: Cr₂O₃-TiO₂; nickel layer; corrosion; cyclic impact; crack evolution



Academic Editor: Frederic Sanchette

Received: 31 December 2024

Revised: 10 January 2025

Accepted: 14 January 2025

Published: 16 January 2025

Citation: Yang, H.; Zhao, Y.; Qin, X.; Jin, Y.; Zhao, X.; Tian, K.; Wang, X.; Zhang, Z. The Damage Evolution of a Cr₂O₃-TiO₂ Coating Subjected to Cyclic Impact and Corrosive Environments and the Influence of a Nickel Intermediate Layer. *Coatings* **2025**, *15*, 98. <https://doi.org/10.3390/coatings15010098>

Copyright: © 2025 by the authors. Licensee MDPI, Basel, Switzerland. This article is an open access article distributed under the terms and conditions of the Creative Commons Attribution (CC BY) license (<https://creativecommons.org/licenses/by/4.0/>).

1. Introduction

Ceramic coatings are well known for their excellent high-temperature stability, thermal shock resistance, wear resistance, and optoelectronic properties, particularly excelling in enhancing the wear and corrosion resistance of components [1–4]. Ceramic coatings have been applied to the surfaces of seawater pump blades and deep-sea combustible ice extraction equipment to prevent erosion caused by seawater and sand particles, which are also widely used on the surfaces of fuel pump rotors, mud pump piston rods, and sucker rod couplings in the petroleum industry to enhance wear and corrosion resistance [5–7]. Cr₂O₃ exhibits exceptional hardness, wear resistance, and pressure tolerance. The incorporation of TiO₂ improves its ductility and toughness, resulting in CT coatings with excellent mechanical properties, making them widely used in demanding service environments [8]. However, defects such as porosity and microcracks in the layers are difficult to avoid. Extensive research has been conducted to investigate the microstructure of plasma-sprayed CT ceramic coatings, with particular attention to crack evolution [9]. However, due to the complexity of the internal structure and interface morphology of transition layers

and ceramic coatings, studying micro dynamic fracture behavior and how to suppress crack propagation has become a major challenge [10]. Consequently, the inclusion of TiO₂ results in the enhanced toughness and corrosion resistance of the coatings, thus exhibiting exceptional physicochemical characteristics [11].

Microcracks and pores are common issues in plasma-sprayed ceramic coatings [12,13], particularly under cyclic stress conditions, where crack propagation occurs below the fracture strength of the coating [14]. The typical mechanisms of crack propagation involve intrasplat cracking, intersplat decohesion, the interlinking of pores and cracks, mutual splat sliding, and pore compaction, leading to coating failure [15]. Plasma-sprayed coatings are often applied in environments with corrosive media, where corrosion initially occurs at the surfaces of partially unmelted particles, pores, and edges of microcracks [16]. The corrosion mechanism of a ceramic coating–metal substrate system can be attributed to three aspects: (i) penetration of electrolyte and corrosive species through interconnected coating pores towards the substrate, (ii) corrosion of the active area along the coating–substrate interface, and (iii) accumulation of corrosion products at the coating–substrate interface, resulting in a reduction in adhesion strength [17]. In engineering applications, stress corrosion cracking is the primary failure mode of thermal-sprayed ceramic coatings. Coating interfacial stress corrosion cracking (ISCC) refers to the delamination, cracking, and fracture of the coating and substrate at the interface due to stress concentration and the combined effects of corrosion [18]. The mismatch in thermal expansion coefficients between the ceramic coating and the substrate material, as well as the presence of micro-voids at the interface, can trigger stress corrosion cracking, particularly when alternating stress and corrosion act synergistically, promoting crack propagation [19–21].

The impeller blades of seawater pumps and valves of marine equipment are often subjected to erosion from seawater and sand particles. The presence of a high concentration of chloride ions, combined with the cyclic stress caused by sand particle impact, can easily lead to the failure of ceramic coatings. There is a lack of research on the damage evolution law of ceramic coatings under corrosive media and impact loads, and determining how to suppress coating–substrate system failure is an important challenge in engineering. This study conducted particle impact experiments in an environment with a large amount of chloride ions present to analyze the damage evolution mechanism of ceramic coatings. The method of using a nickel layer as a transition layer for the ceramic coating was proposed to investigate the effects of the Ni layer on corrosion potential and current, and to analyze its impact on interface crack propagation. This research holds significant importance for enhancing the service life of ceramic coatings subjected to impact loads in corrosive environments.

2. Experiments

2.1. The Preparation of CT Coatings

In this study, CT coatings with and without a Ni interlayer were prepared on 304 stainless steel using the XM-300SK (Shanghai Xiuma Spraying Machinery, Shanghai, China) supersonic plasma spraying system. The substrate used for this plasma spray was 304 stainless steel with a size specification of 100 × 100 × 3 mm³. The primary gases and powder carrier gases employed in the system were argon. The transition layer was composed of Ni powders with a particle size of 30–100 μm. TiO₂ accounts for 60% of the total mass of the ceramic powder. The process parameters for CT and the transition layer are shown in Table 1.

Table 1. Plasma process parameters.

Process Parameters	Ni Layer	Ceramic Layer
Current/A	300	500
Voltage/V	62	80
Plasma gas flow (Ar)/L·min ⁻¹	60	60
Plasma gas flow (H ₂)/L·min ⁻¹	10	15
Spray distance (mm)	100	100
Powder feed rate (g/min)	30	30

2.2. Corrosion and Electrochemical Experiments

The CT coating samples after spraying were cut into small pieces of $10 \times 10 \times 3 \text{ mm}^3$ using a wire cutting machine. After cutting the samples, the cut surfaces were polished and immersed in 5% HCl at room temperature for 1 h to investigate the corrosion behavior of the coating, Ni layer, substrate, and interface. The electrochemical corrosion behaviors were studied by potentiodynamic polarization spectroscopy. Before the experiment, the samples were polished first. The polishing liquid used was a suspension of alumina particles. All the electrochemical experiments were conducted on an electrochemical station (Versa Studio: PARSTAT 3000 A-DX, Berwyn, PA, USA), as shown in Figure 1II. The cell used was a typical three-electrode one fitted with a platinum sheet measuring $1 \times 1 \times 0.05 \text{ cm}^3$ as the counter electrode (CE), working electrode (specimen) and saturated calomel electrode (SCE) as the reference electrode (RE). The open circuit potential (E_{corr}) and corrosion current density (I_{corr}) of the samples, with and without the Ni layer, were analyzed through electrochemical experiments.

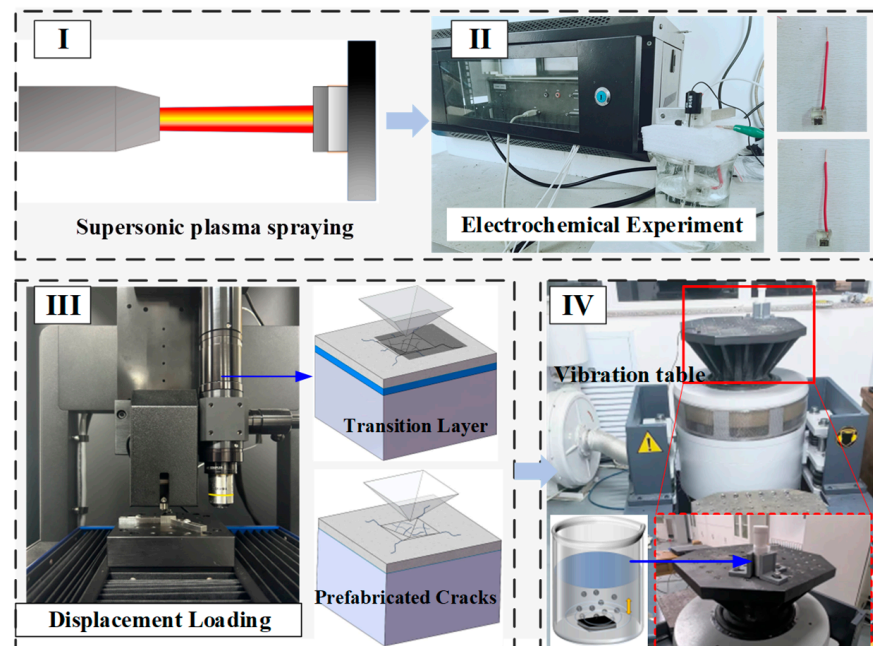


Figure 1. The process of experiments: (I) supersonic plasma spraying; (II) electrochemical experiments; (III) displacement loading experiment; (IV) impact experiments in corrosive media.

2.3. Crack Prefabrication

To further study the effect of the Ni layer on interface crack propagation, the Micro-Nano mechanical testing system was used to pre-create indentations and cracks on the ceramic coating surface (Figure 1III). The diamond indenter stayed in situ for 20 s after applying a load of 20 N, forming a diamond indentation on the surface of the coating, and forming cracks in the indentation and at sharp corners.

2.4. Cyclic Impact Experiment in Corrosive Media

To explore the damage evolution of the ceramic coating, a cyclic impact test in a corrosive environment was conducted. The sample was fixed at the bottom of the polytetrafluoroethylene test tube (Figure 1IV), 50 SiC balls with a diameter of 3 mm were added into the test tube, and 5% hydrochloric acid was also added as the corrosion medium. The test tube was installed on the shaking table, and a vibration with an amplitude of 0.5 mm and a frequency of 20 Hz was applied for 2 h. The synergistic effect of cyclic impact stress generated by SiC balls and corrosive media induces the propagation of pre-existing cracks on ceramic coatings.

2.5. Characterization Techniques

After polishing the surface of the coatings, the samples' microstructures were characterized using a scanning electron microscope (SEM, Merlin Compact, Zeiss, Jena, Germany), and the element distribution was examined using energy-dispersive spectroscopy (EDS). The phase composition of the ceramic coatings and substrates was tested using an X-ray diffractometer (XRD, Ultimate IV, RIGAKU, Tokyo, Japan), and the test results were analyzed using MDI Jade 6 software (V.6, ICDD, Philadelphia, PA, USA). Additionally, a simulation was performed to investigate the stress variation pattern in the coatings and analyze the formation mechanism of residual stresses.

3. Results and Discussion

3.1. Microscopic Characteristics of CT Coating–Substrate System

In addition to the abundant presence of chromium (Cr) and nickel (Ni), there are mineral phases of Taenite FeNi and FeNi₃ compound phases in the matrix, which can be confirmed by the X-ray diffraction patterns. The appearance of these two phases is attributed to the mutual dissolution, diffusion and reaction between iron and nickel during the heat treatment of the substrate. The internal structure of the coating shown in Figure 2b reveals the presence of Cr₂O₃ and TiO₂, indicating a typical plasma-sprayed ceramic coating. The addition of titanium oxide provides a certain level of toughness to inhibit crack propagation within the coating [22].

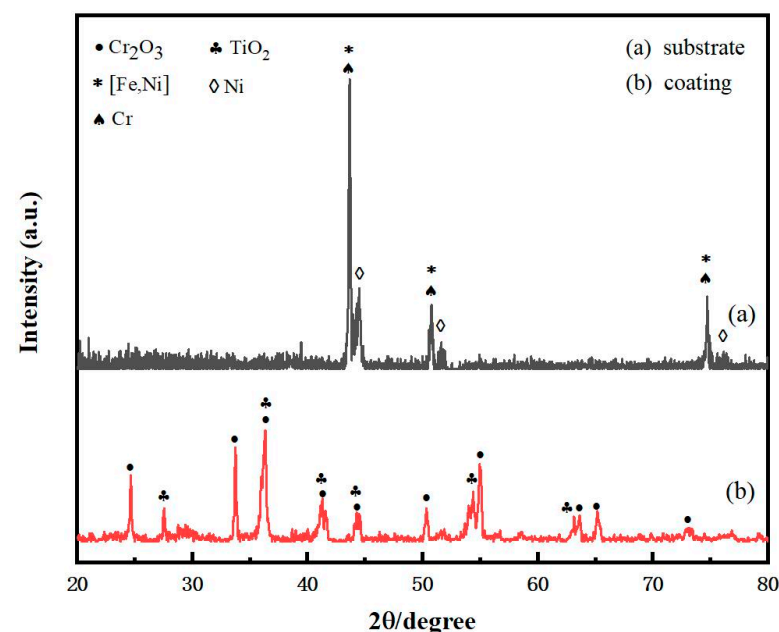


Figure 2. XRD patterns: (a) substrate; (b) coating.

Powder particles are exposed to high temperatures and kinetic energy through high-pressure gases and heating. When colliding with the substrate surface, the powder particles form a molten or semi-molten splash. These deformed particles intertwine and stack together in a wave-like pattern, forming a layered microstructure, as illustrated in Figure 3a. During the stacking process, the changes in particle flight velocity and temperature triggered the coating structure to show significant irregularities, resulting in gaps or voids between the stacked particles. The elemental distribution map clearly reveals distinct regions and boundaries for Cr and Ti, corresponding to the distribution regions of the particles. The elemental distribution maps clearly show the different regions and boundaries of Cr and Ti, corresponding to the distribution areas of the particles, where the O intensity is significantly higher in the Cr region, indicating higher oxygen content in this region (Figure 2b). The presence of pores and microcracks is commonly observed in ceramic coatings. During plasma spraying, pores and microcracks can be generated from different sources, such as entrapped gases, the incomplete filling in of the rapidly solidifying splats, the shrinking of the splats during rapid solidification, etc. Additionally, as the temperature of deforming particles decreases, they undergo shrinkage. Failure to replenish the liquid phase in a timely manner can also result in the formation of voids within the coating [23–25].

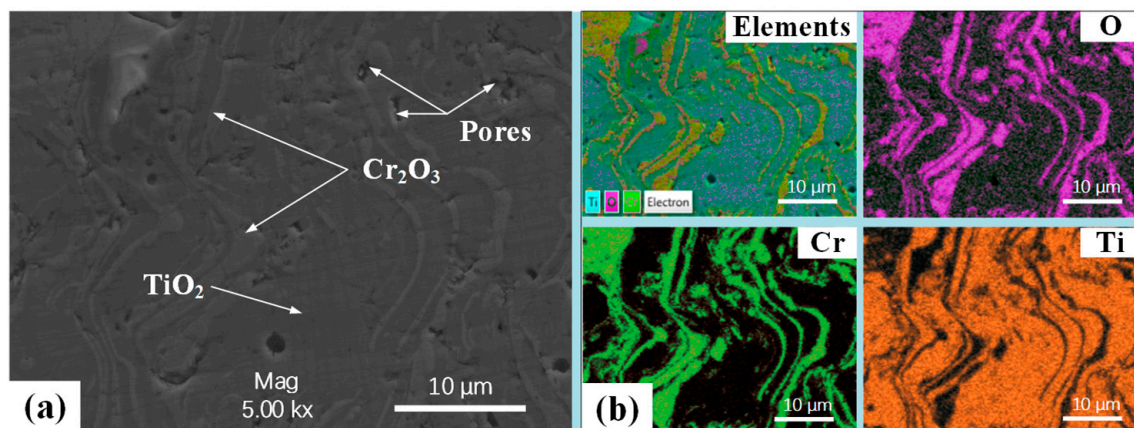


Figure 3. CT coating: (a) microstructure of CT coating; (b) element distribution.

As shown in Figure 4a, the coating–substrate system was observed to be clearly divided into three parts: the substrate, the transition layer, and the coating. Interface 1 and Interface 2 were formed between the nickel layer, ceramic coating, and substrate, achieving a strong bond between the materials. The elemental distribution of the coating–substrate system was investigated using energy-dispersive X-ray spectroscopy (EDS, Zeiss Merlin Compact, Zeiss, Jena, Germany), revealing distinct separation into three different regions. The transition layer served to bind the coating and the substrate, and was mainly composed of nickel. However, the EDS spectrum reveals the presence of Al and O in the transition layer, which is attributed to the retention of alumina particles during metallographic polishing. The ceramic coating primarily contained elements such as Cr, Ti, and O. The substrate was mainly composed of elements such as Fe and Ni. Figure 4b shows numerous black particles embedded in the transition layer. EDS analysis identifies these black particles as corresponding to aluminum elements, confirming that they are alumina abrasive particles embedded in the nickel layer.

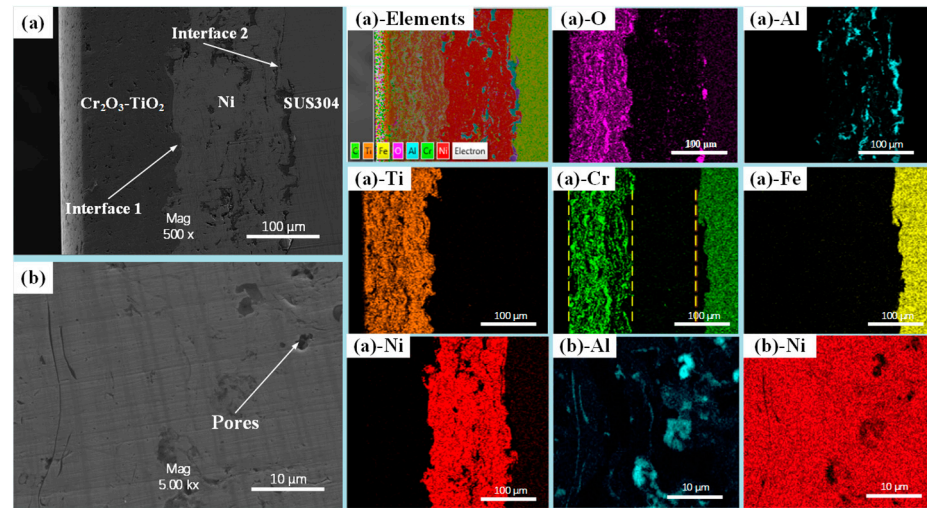


Figure 4. Coating–substrate system and element distribution: (a) ceramic coating with transition layer; element distribution (b) transition layer; element distribution.

3.2. Interfacial Crack Formation

To investigate the mechanism by which a nickel layer influences the interfacial cracking of CT coatings, two types of coating–substrate systems were prepared using plasma spraying technology. In the first type of sample, the CT coating was directly sprayed onto the 304 stainless steel. In the second type, a nickel layer was deposited between the substrate and the CT coating. The coating exhibited numerous pores, with a particularly high density of pores and microcracks at the interface, as shown in Figure 5a. This phenomenon occurred because, upon the impact of a droplet on a solid surface, a thin air film forms between the center of the droplet and the substrate. This air film ultimately evolves into a spherical bubble to minimize surface energy, resulting in the formation of pores at the interface [25]. Additionally, during the cooling process, thermal stresses arise at the interface due to the different thermal expansion coefficients. These stresses generate interface cracks originating from defects such as pores [26]. The samples were placed in a 5% HCl solution for a corrosion period of 2 h at room temperature. As shown in Figure 5b, corrosion occurred at the interface between the substrate and the coating. The corrosion traces on the substrate exhibited a striped pattern, while pronounced continuous cracks were observed at the interface. This confirms that the interface is the most vulnerable part of the thermal-sprayed coating in a corrosive environment, and corrosion-induced cracking at the interface is an important reason for the failure of the thermal-sprayed coating. Elemental distribution analysis reveals the presence of elements such as O, Cr, and Ti in the coating, while showing that the substrate predominantly contains Fe. A clear demarcation is observed between the coating and the substrate.

Corrosion experiments on samples with a nickel layer revealed that the nickel layer and ceramic coating were well bonded, with no cracks observed at Interface 1. However, significant cracks were found at Interface 2, between the nickel layer and the substrate, as shown in Figure 6a. Figure 6b,c show numerous pores in both the ceramic coating and the nickel layer. Interface 1 is clearly identified and surrounded by many defects. Obvious corrosion cracks were formed at Interface 2, and obvious β -phase corrosion occurred on the substrate. However, there were fewer corrosion marks on the ceramic coating and nickel layer, and slight intergranular corrosion was observed on the nickel layer (Figure 6d–f). As shown in Figure 6j, elemental distribution indicates that the transition layer is predominantly composed of nickel, while aluminum is introduced from alumina abrasive particles in the polishing solution. The ceramic coating depicted in Figure 6i contains elements such as Ti, Cr, and O, indicating that it is a corrosion-resistant ceramic.

The intermediate layer is primarily composed of nickel, while the aluminum element is introduced from the alumina abrasive particles in the polishing solution (Figure 6j). The enhanced corrosion resistance at Interface 1 inhibits the growth of interfacial cracks, while the cracks at Interface 2 are formed due to the corrosion of the substrate near the interface.

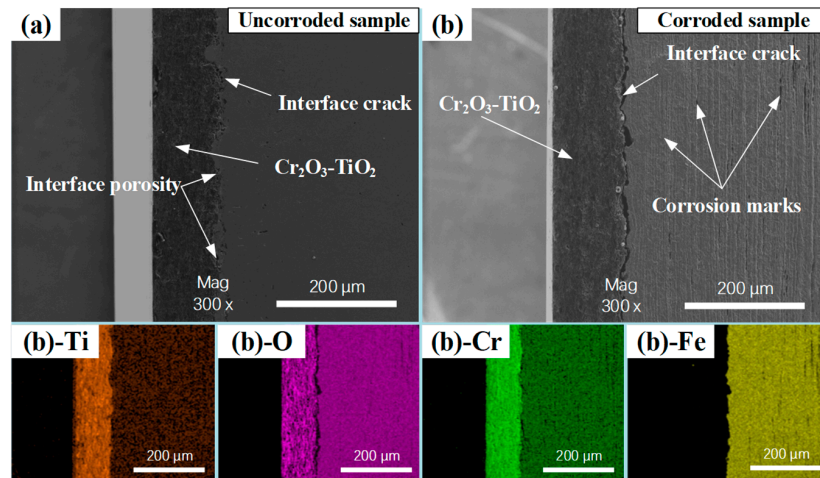


Figure 5. Corrosion cracking of the coating interface: (a) uncorroded sample; (b) corroded sample and its element distribution.

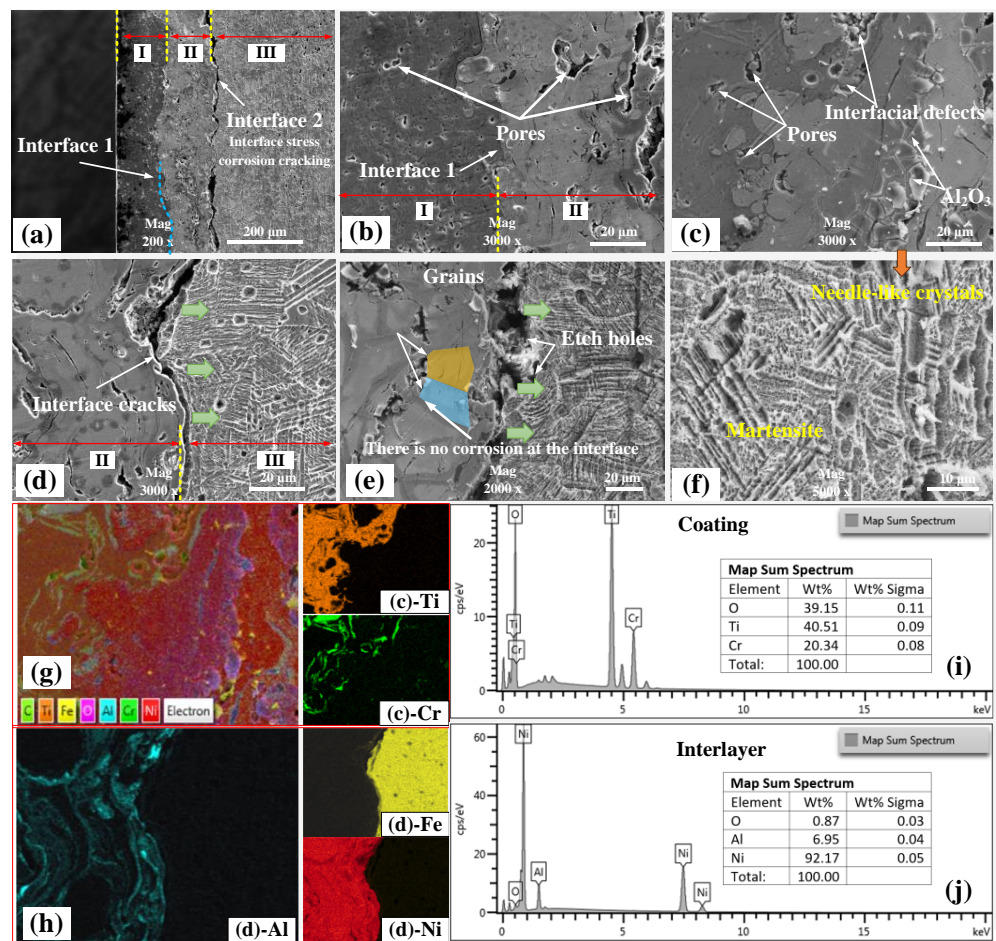


Figure 6. Corrosion behavior of the coating–substrate system with a nickel layer: (a) CT/Ni/Substrate; (b) Interface 1; (c) Interface 1. Interfacial defects: (d) interface crack; (e) corrosion around the cracks; (f) corrosion of the substrate; (g) element distribution. Interface 1 (h) element distribution; Interface 2 (i) EDS energy spectrum; coating (j) EDS energy spectrum; substrate.

3.3. Electrochemical Characteristics

To evaluate the corrosion resistance of CT/Ni/Substrate and CT/Substrate, Tafel curves of the two samples were obtained using an electrochemical workstation. As depicted in Figure 7, the passivation region of the sample with the added nickel layer is more pronounced compared to that of the CT/Substrate sample, indicating the easier formation of a passive film and enhanced corrosion resistance. Furthermore, the corrosion potential of the CT/Ni/Substrate sample increased from -0.657 V to -0.766 V, and the corrosion current density decreased from 9.197×10^{-6} A/cm² to 8.088×10^{-6} A/cm². The negative shift in potential is merely a thermodynamic tendency. The decrease in current density demonstrates the enhanced corrosion resistance of the CT/Ni/Substrate sample. Additionally, the passivation region of the CT/Ni/Substrate samples was significantly enlarged, indicating that the incorporation of the Ni layer facilitates the formation of a passivation film on the surface, thereby enhancing the passivation phenomenon.

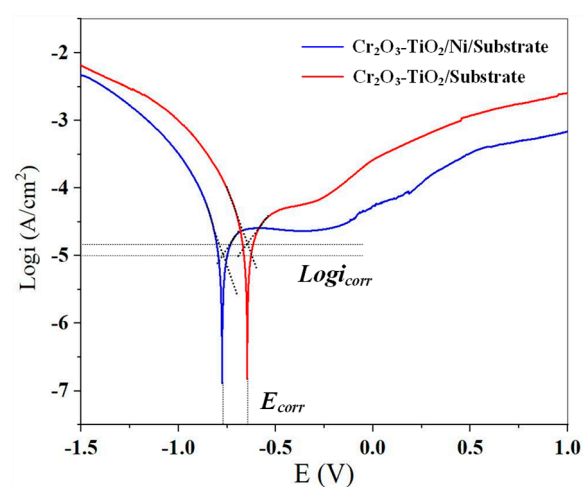


Figure 7. Polarization curve of CT/Ni/Substrate and CT/Substrate.

3.4. Damage Evolution of the Coating–Substrate System

Vibrations with a frequency of 20 Hz and an amplitude of 0.5 mm were generated using a vibration table, causing SiC particles to repeatedly impact the ceramic coating surface in a 5% hydrochloric acid solution. Figure 8a illustrates two types of failure modes occurring on the coating surface. Cracking is a common and almost unavoidable failure mode for ceramic coatings, especially under the combined effects of corrosive media and cyclic stress, leading to crack propagation on the surface. As cracks propagate, corrosion continues within the crack gaps, which is associated with stress corrosion cracking. The susceptibility to stress corrosion cracking is significantly higher than it is under non-corrosive or non-stress conditions [27–29]. Figure 8d shows corrosion and minor spalling on both sides of the cracks. The other form of damage is the localized spalling of the coating, manifested as the layer-by-layer delamination of the ceramic coating, initiated by defects such as pores, eventually forming deep pits on the coating surface, as depicted in Figure 8b,c.

To further investigate the damage evolution patterns of the film–substrate system, indents and pre-cracks were prepared on two samples: CT/Ni/Substrate and CT/Substrate. The displacement–load curves of the two samples are similar. However, under the same applied load of 20 N, the displacement of the CT/Ni/Substrate sample is generally larger than that of the CT/Substrate sample (Figure 9). This is because when the indentation depth exceeds 1/10 of the coating thickness, the resulting displacement–load curve represents the film–substrate system rather than the ceramic coating alone. The nickel layer exhibits

good plasticity, leading to more significant deformation under the same load conditions. Consequently, the indentation depth is slightly deeper.

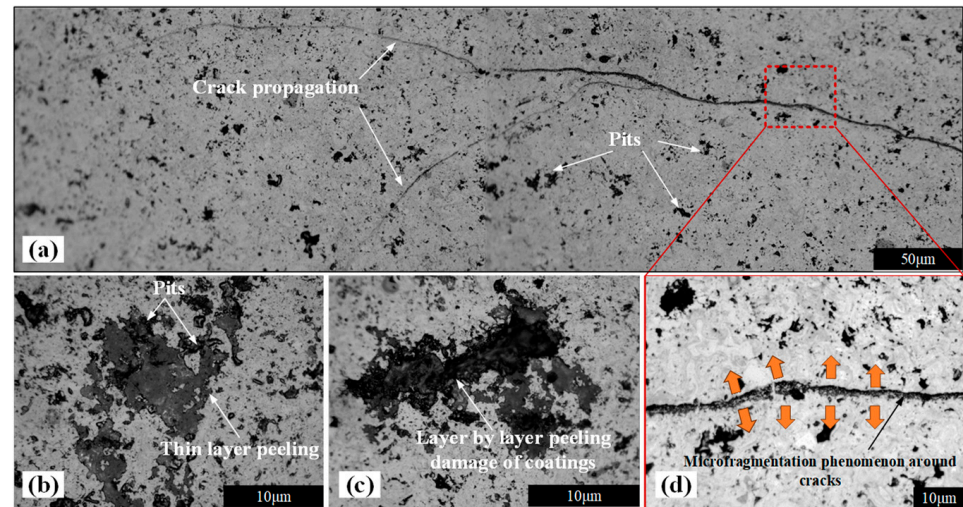


Figure 8. Surface damage forms of CT coatings.

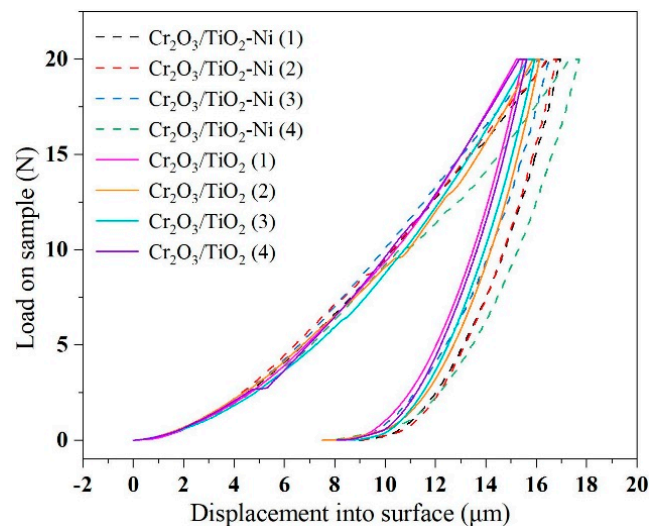


Figure 9. Displacement-load relationship curve.

The indenter of the Micro-Nano mechanical testing system induces two types of damage: indentations and cracks. Figure 10aI shows the indentation of the CT/Ni/Substrate sample, where cracks are generated at the sharp corners of the indentation, and there is slight spalling of the coating at the edges. As the corrosion medium impact experiment progresses, the spalled area of the coating increases, and the cracks within the indentation interweave in a spiderweb-like pattern (Figure 10b2). After 2 h of the corrosion impact experiment, localized delamination of the coating within the indentation occurs, as shown in Figure 10aIII. Figure 10b1 displays the indentation of the CT/Substrate sample. Without the nickel layer, the ceramic coating is more prone to cracking and large-scale delamination. This phenomenon is likely related to the internal stress within the coating and the bonding strength between the film and the substrate. As the impact experiment continues, delamination begins within the coating, and extensive delamination occurs around the warped coating (Figure 10b2). Without a nickel layer as a barrier, the interaction of the corrosion medium and abrasive particles results in the almost complete peeling of the coating within the indentation, deepening the corrosion and continuously increasing the peeling area.

These observations indicate that the presence of the nickel layer effectively suppresses the deterioration of the coating damage.

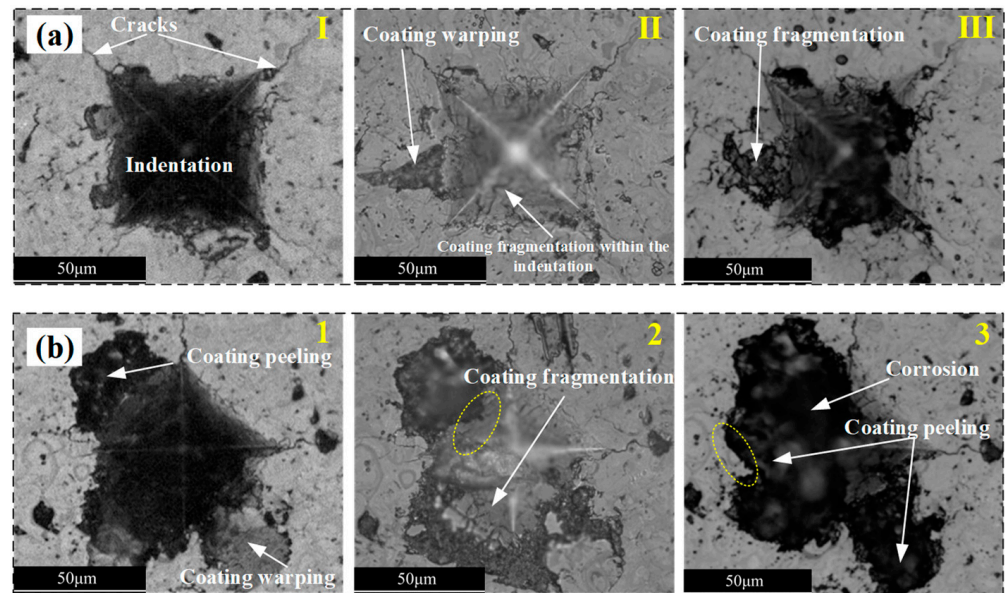


Figure 10. Prefabricated damage and its evolution patterns in a corrosive impact environment: (a) CT/Ni/Substrate; (b) CT/Substrate.

The phenomenon of cracking induced by the combined effect of lower stress (below the fatigue strength) and a mild corrosive environment is referred to as stress corrosion cracking. If only one factor, either stress or the corrosive medium, is present, failure does not occur. However, when both factors act together, cracking can occur rapidly [30]. Stress corrosion leads to a reduction in fracture toughness, which is attributed to the presence of corrosive media. These media attack interlayer bonding and weaken the bond energy of closely connected chemical bonds, thereby causing damage to the crack tip model and initiating rapid crack propagation. Stress plays a crucial role in crack propagation [31]. As shown in Figure 11a, the stress base along the X-axis and Y-axis exhibits tensile stress, while compressive stress is generated within the coating. In the Z-axis direction, tensile stress is present in the areas with the coating. After the introduction of the Ni layer, the stress within both the substrate and the coating decreases; however, stress concentration is observed in the X-axis direction of the Ni layer, and compressive stress is present in the Z-axis direction. In Figure 11b, the CT/Ni/Substrate sample coating exhibits compressive stress in the X-axis direction, which is lower than that of the CT/Substrate sample. The maximum tensile stress occurs at Interface 2, and it is significantly lower than that of the CT/Substrate sample. The presence of the Ni layer transforms the stress in the Z-axis direction from tensile to compressive (Figure 11c). The formation of interfacial cracks aligns with the stress concentration at Interface 2. The development of compressive stress within the CT/Ni/Substrate sample coating and the overall reduction in stress contribute to fewer cracks within the coating, as illustrated in Figure 11b.

The combined effects of corrosive media corrosion and the cyclic impact of SiC balls induce the formation of cracks in ceramic coatings. The propagation of these cracks occurs in two forms: one is parallel to the coating surface, leading to the layer-by-layer spalling of the ceramic coating, and the another form is a through-thickness crack, characterized by its extension towards the coating–substrate interface, as illustrated in Figure 12a. The corrosive medium infiltrates the membrane–substrate interface through capillary action via cracks generated during fatigue cycles or pores in the surface coating of the sample, leading

to the formation of corrosion pits. Subsequently, these pits initiate and propagate cracks within the substrate [32,33]. The micromechanical system generates surface cracks, which progressively extend towards the interface under the repeated impacts of the corrosive media and SiC balls. When the cracks reach the interface, they provide a pathway for the corrosive media, resulting in stress corrosion cracking at the interface [34], as shown in Figure 12b. Figure 12d reveals that the substrate is preferentially corroded by the media, and the occurrence of interface cracks depends on the substrate’s corrosion resistance. After the addition of a nickel layer (Figure 12c), when the cracks extend to the interface, the corrosive media contact the nickel layer, inhibiting corrosion and making it difficult for interface cracks to form (Figure 12c,e,f). Furthermore, the presence of the nickel layer effectively reduces the stress at the interface, significantly enhancing the suppression of stress corrosion cracking at the interface. Consequently, the constructed CT/Ni/304 stainless steel coating–substrate system exhibits excellent performance in suppressing damage evolution under corrosive media and repeated impact conditions.

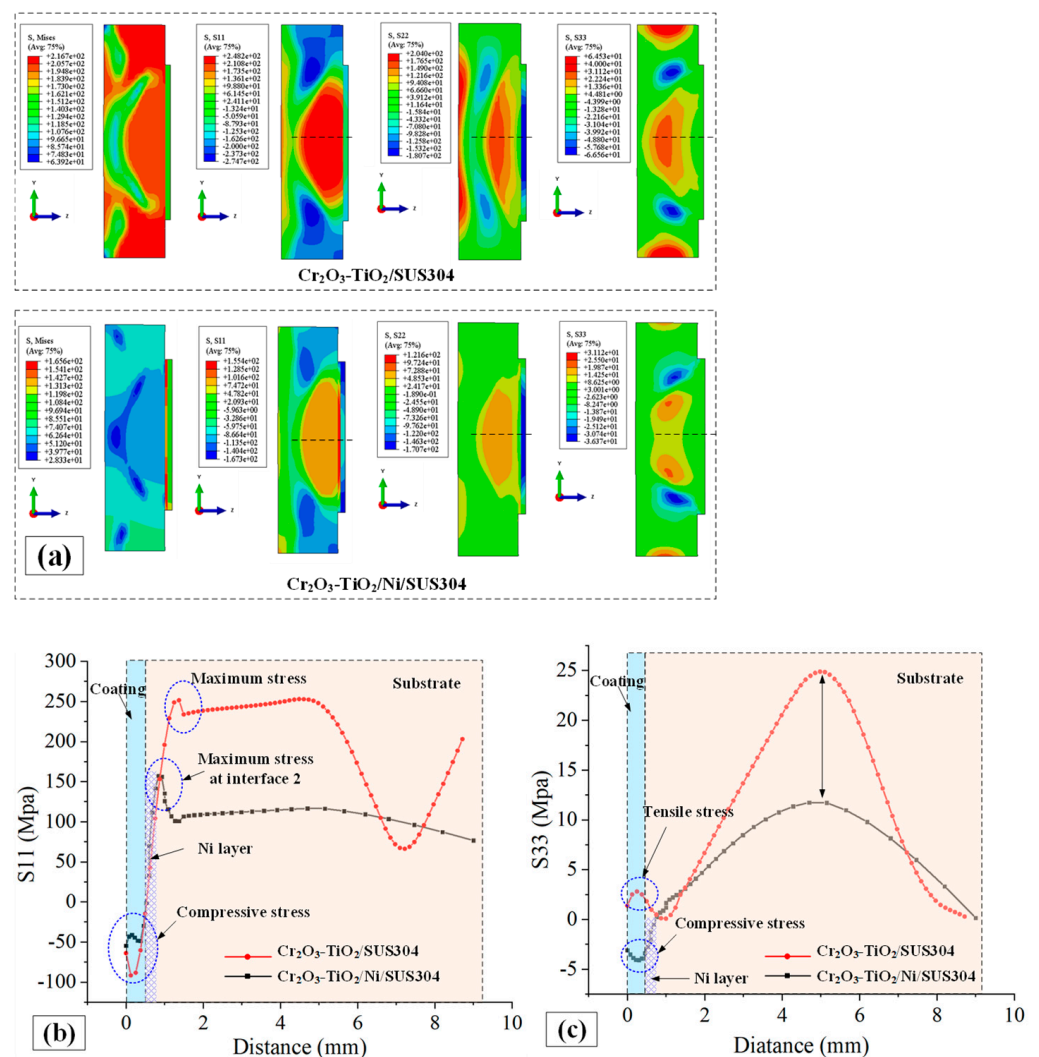


Figure 11. Stress distribution characteristics. (a) Stress cloud maps of two samples: (b) S11 and (c) S33.

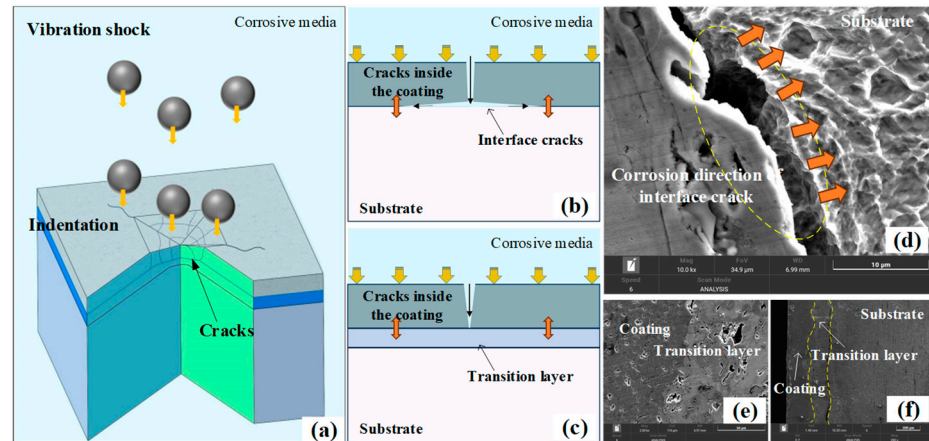


Figure 12. Damage evolution in corrosive and impact environments: (a) damage generation; (b) CT/Substrate; (c) CT/Ni/Substrate; (d) interface cracks; (e) interface between nickel layer and ceramic coating; (f) CT/Ni/Substrate.

4. Conclusions

To enhance the suitability of plasma-sprayed ceramic coatings under corrosive impact conditions, this study deposited a nickel layer between the ceramic coating and 304 stainless steel. The findings demonstrate that the nickel layer reduces interfacial and coating stresses, suppresses the propagation of interfacial cracks, and effectively improves the damage resistance of the ceramic coating.

- (a) The formation of interfacial cracks primarily depends on the corrosion resistance of the materials on either side of the interface. Therefore, the addition of a nickel layer effectively inhibits the formation of cracks between the ceramic coating and the nickel layer. However, it cannot prevent the formation of cracks between the nickel layer and the substrate, which is due to the substrate's poor corrosion resistance.
- (b) The nickel layer reduces the stress on the coating and substrate, but stress concentration occurs near the interface between the nickel layer and substrate. The stress in the Z-axis direction changes from tensile stress to compressive stress.
- (c) The presence of the nickel layer enhances the corrosion resistance of the coating–substrate system and strengthens the passivation phenomenon. The corrosion potential of the CT/Ni/Substrate sample increased from -0.657 V to -0.766 V, and the corrosion current density decreased from 9.197×10^{-6} A/cm² to 8.088×10^{-6} A/cm².
- (d) The combined effects of corrosion and impact result in two types of damage on the surface of ceramic coatings: through-thickness cracks and corrosion pits. Through-thickness cracks are the primary cause of interfacial cracks, while corrosion pits arise from the progressive delamination of the ceramic coating layers.

Author Contributions: H.Y.: methodology, experiment, data curation, and writing—original draft. Y.Z.: experiment, writing—review and editing. X.Q.: simulation. Y.J.: writing—review and editing. X.Z.: experiment. K.T.: investigation and simulation. X.W.: methodology. Z.Z.: conceptualization and supervision. All authors have read and agreed to the published version of the manuscript.

Funding: This project was supported by National Natural Science Foundation of China (Grant No. 52305510), National Defense Science and Technology Key Laboratory (6142005KJW2022011) and Natural Science Foundation of Shandong Province (ZR2023QE044).

Data Availability Statement: All data and material are presented in the main manuscript and additional supporting files are available from corresponding author on reasonable request.

Conflicts of Interest: The authors declare that they have no conflicts of interest.

References

1. Han, C.; Wang, Z.; Ma, L.; Huang, G.; Ma, Y. Cold spray for ceramic metallisation: A review. *Adv. Appl. Ceram.* **2021**, *120*, 358–380. [[CrossRef](#)]
2. Missner, M.; Stryhalski, J.; Tomiyama, M.; Soares, P.; Recco, A.; Fontana, L. Rutile TiO₂ thin films growth on glass substrates with generation of high entropy interface. *J. Mater. Res. Technol.* **2023**, *24*, 963–970. [[CrossRef](#)]
3. Talavari, F.; Shakeri, A.; Mighani, H. Synthesis of Cr₂O₃/TiO₂ nanocomposite and its application as the blocking layer in solar cells. *J. Environ. Anal. Chem.* **2018**, *5*, 2380–2391. [[CrossRef](#)]
4. Dey, A.; Banerjee, K.; Mukhopadhyay, A.K. Microplasma sprayed hydroxyapatite coating: Emerging technology for biomedical application. *Mater. Technol.* **2014**, *29*, 15–20. [[CrossRef](#)]
5. Zhang, H.; Wang, Y.; Chen, X.; Zhang, Z.; Zeng, X.; Cheng, X. Corrosion behaviors of Al₂O₃–20TiO₂ and Cr₂O₃–3TiO₂–5SiO₂ coatings in both artificial seawater and high-pressure hydrogen sulfide seawater. *Ceram. Int.* **2024**, *50*, 34346–34356. [[CrossRef](#)]
6. Lakshmi, K.P.J.; Irappa, S.; Raghavendra, C.R.; Basavarajappa, S. High temperature erosive behaviour of plasma sprayed NiCrAlY/B4C/Cenospherecoating on MDN 321 turbine steel. *Int. J. Surf. Eng. Coat.* **2023**, *101*, 49–56.
7. Zavareh, M.A.; Sarhan, A.A.D.M.; Karimzadeh, R.; Singh, R.S.A. Analysis of corrosion protection behavior of Al₂O₃-TiO₂ oxide ceramic coating on carbon steel pipes for petroleum industry. *Ceram. Int.* **2018**, *44*, 5967–5975. [[CrossRef](#)]
8. Vernhes, L.; Bekins, C.; Lourdel, N.; Poirier, D.; Lima, R.S.; Li, D.; Klemberg-Sapieha, J.E. Nanostructured and conventional Cr₂O₃, TiO₂, and TiO₂-Cr₂O₃ thermal-sprayed coatings for metal-seated ball valve applications in hydrometallurgy. *J. Therm. Spray Technol.* **2016**, *25*, 1068–1078. [[CrossRef](#)]
9. Rasooli, A.; Safavi, M.S.; Hokmabad, M.K. Cr₂O₃ nanoparticles: A promising candidate to improve the mechanical properties and corrosion resistance of Ni-Co alloy coatings. *Ceram. Int.* **2018**, *44*, 6466–6473. [[CrossRef](#)]
10. He, X.; Song, P.; Huang, T.; Wan, F.; Kong, D.; Zhai, R.; Hua, C.; Dai, J. Fracture process simulation and crack resistance behavior analysis of transition-layer ceramic coating based on real image reconstruction model. *Surf. Interfaces* **2024**, *46*, 104003. [[CrossRef](#)]
11. Babu, P.S.; Sen, D.; Jyothirmayi, A.; Krishna, L.R.; Rao, D.S. Influence of microstructure on the wear and corrosion behavior of detonation sprayed Cr₂O₃-Al₂O₃ and plasma sprayed Cr₂O₃ coatings. *Ceram. Int.* **2018**, *44*, 2351–2357. [[CrossRef](#)]
12. Wang, S.; Liu, X.; Zhang, J.; Xu, P.; Wei, M.; Liu, G.; Zhan, X.; Coyle, T.W.; Mostaghimi, J. Tailoring the wetting behaviors and surface structures of yttrium oxide coatings deposited via different plasma spray processes. *J. Mater. Res. Technol.* **2024**, *29*, 1924–1936. [[CrossRef](#)]
13. Ahmadian, S.; Jordan, E.H. Explanation of the effect of rapid cycling on oxidation, rumpling, microcracking and lifetime of air plasma sprayed thermal barrier coatings. *Surf. Coat. Technol.* **2014**, *244*, 109–116. [[CrossRef](#)]
14. Kovářik, O.; Haušild, P.; Medřický, J.; Tomek, L.; Siegl, J.; Mušálek, R.; Curry, N.; Björklund, S. Fatigue Crack Growth in Bodies with Thermally Sprayed Coating. *J. Therm. Spray Technol.* **2016**, *25*, 311–320. [[CrossRef](#)]
15. Mušálek, R.; Kovářik, O.; Matějček, J. In-situ observation of crack propagation in thermally sprayed coatings. *Surf. Coat. Technol.* **2010**, *205*, 1807–1811. [[CrossRef](#)]
16. Huang, B.; Wang, J.; Tang, Z.-H.; Li, W.-D.; Zhu, W.-J.; Gu, R.-B. Fluoride-mediated corrosion mechanism of atmospheric-plasma-sprayed yttrium-aluminium garnet ceramic coatings. *J. Eur. Ceram. Soc.* **2022**, *42*, 6146–6158. [[CrossRef](#)]
17. Zamani, P.; Valefi, Z.; Jafarzadeh, K. Comprehensive study on corrosion protection properties of Al₂O₃, Cr₂O₃ and Al₂O₃-Cr₂O₃ ceramic coatings deposited by plasma spraying on carbon steel. *Ceram. Int.* **2022**, *48*, 1574–1588. [[CrossRef](#)]
18. Chen, W.; Hu, T.; Wang, C.; Xiao, H.; Meng, X. The effect of microstructure on corrosion behavior of a novel AlCrTiSiN ceramic coating. *Ceram. Int.* **2020**, *46*, 12584–12592. [[CrossRef](#)]
19. Zhang, Z.; Zhong, X.; Li, L.; Hu, J.; Peng, Z. Unmasking the delamination mechanisms of a defective coating under the co-existence of alternating stress and corrosion. *Prog. Org. Coat.* **2023**, *180*, 107560. [[CrossRef](#)]
20. Ozkan, D. Structural characteristics and wear, oxidation, hot corrosion behaviors of HVOF sprayed Cr₃C₂-NiCr hardmetal coatings. *Surf. Coat. Technol.* **2023**, *457*, 129319. [[CrossRef](#)]
21. Wang, Z.; Zhang, J.; Liu, X.; Liu, J.; Liu, G. Failure mechanism of plasma sprayed Tb-YSZ coating under NaCl high-low temperature cyclic corrosion. *Surf. Coat. Technol.* **2023**, *456*, 129244. [[CrossRef](#)]
22. Hanifi, D.; Hakimi, N.; Ali, R.; Huang, T.; Huma, T.; Bakhshyar, D.; Afzali, N.R.; Shafi, M.; Babeker, H.; Lu, J.; et al. The fracture toughness and tribological performance of NiAl/Al₂O₃-40 Wt.% TiO₂ coating generated by air plasma spraying. *Ceram. Int.* **2024**, *50*, 1533–1546. [[CrossRef](#)]
23. Thirumalaikumarasamy, D.; Shanmugam, K.; Balasubramanian, V. Effect of atmospheric plasma spraying parameters on porosity level of alumina coatings. *Surf. Eng.* **2012**, *28*, 759–766. [[CrossRef](#)]
24. Ctibor, P.; Lechnerová, R.; Beneš, V. Quantitative analysis of pores of two types in a plasma-sprayed coating. *Mater. Charact.* **2006**, *56*, 297–304. [[CrossRef](#)]
25. Shukla, R.K.; Kumar, A.; Kumar, R.; Singh, D.; Kumar, A. Numerical study of pore formation in thermal spray coating process by investigating dynamics of air entrapment. *Surf. Coat. Technol.* **2019**, *378*, 124972. [[CrossRef](#)]

26. Ferguen, N.; Leclerc, W.; Lamini, E.-S. Numerical investigation of thermal stresses induced interface delamination in plasma-sprayed thermal barrier coatings. *Surf. Coat. Technol.* **2023**, *461*, 129449. [[CrossRef](#)]
27. Terán, G.; Capula-Colindres, S.; Velázquez, J.; Zuñiga-Hinojosa, M.; Contreras, A. Modeling 3D finite element analysis of a semi-elliptical crack on stress corrosion cracking of API X52 pipeline. *Forces Mech.* **2024**, *16*, 100279. [[CrossRef](#)]
28. Han, C.; Yu, M.; Jia, X.; Zhao, Z.; Zhang, C.; Xiao, J.; Li, S.; Liu, J. Effect of inhomogeneous microstructures on stress corrosion cracking sensitivity of 2050-T84 Al-Li alloy thick plate. *Corros. Sci.* **2024**, *235*, 112213. [[CrossRef](#)]
29. Wei, Z.-Y.; Cai, H.-N. Stress states and crack behavior in plasma sprayed TBCs based on a novel lamellar structure model with real interface morphology. *Ceram. Int.* **2019**, *45*, 16948–16962. [[CrossRef](#)]
30. Loto, C.A. Stress corrosion cracking: Characteristics, mechanisms and experimental study. *Int. J. Adv. Manuf. Technol.* **2017**, *93*, 3567–3582. [[CrossRef](#)]
31. Zhang, W.; Sun, J.; Ding, D.; Hou, D. Nanoscale insights on the stress corrosion mechanism of calcium-silicate-hydrate. *J. Build. Eng.* **2023**, *80*, 107991. [[CrossRef](#)]
32. Tokaji, K.; Ogawa, T.; Hwang, J.U.; Kobayashi, Y.; Harada, Y. Corrosion Fatigue Behavior of a Steel with Sprayed Coatings. *J. Therm. Spray Technol.* **1996**, *5*, 269–276. [[CrossRef](#)]
33. Morelli, S.; Bursich, S.; Testa, V.; Bolelli, G.; Micciché, A.; Lusvarghi, L. CMAS corrosion and thermal cycling fatigue resistance of alternative thermal barrier coating materials and architectures: A comparative evaluation. *Surf. Coat. Technol.* **2022**, *439*, 128433. [[CrossRef](#)]
34. Cai, H.; Shan, X.; Lu, J.; Luo, L.; Cai, Z.; Wang, W.; Zhang, X.; Zhao, X. The crack behavior and delamination mechanisms of air plasma sprayed thermal barrier coatings under ultrasonic plasma jet at 1600 °C. *J. Eur. Ceram. Soc.* **2023**, *43*, 4136–4145. [[CrossRef](#)]

Disclaimer/Publisher’s Note: The statements, opinions and data contained in all publications are solely those of the individual author(s) and contributor(s) and not of MDPI and/or the editor(s). MDPI and/or the editor(s) disclaim responsibility for any injury to people or property resulting from any ideas, methods, instructions or products referred to in the content.